High-resolution imaging of lowermost mantle structure under the Cocos plate

Christine Thomas
Department of Earth and Ocean Sciences, University of Liverpool, Liverpool, UK

Edward J. Garnero
Department of Geological Sciences, Arizona State University, Tempe, Arizona, USA

Thorne Lay
Earth Sciences Department and Institute of Geophysics and Planetary Physics, University of California, Santa Cruz, California, USA

Received 6 February 2004; revised 21 May 2004; accepted 14 June 2004; published 12 August 2004.

[1] Broadband seismic shear waves are analyzed to investigate the fine-velocity structure in the lowermost mantle beneath the Cocos plate, a region where previous studies have indicated the presence of a shear velocity increase about 200–300 km above the core-mantle boundary. Data from 14 South American earthquakes recorded at California broadband networks provide dense ray path sampling of the lowermost mantle in an approximately 700 km long north-south corridor, roughly 150 km wide. Application of a simplified seismic migration method that uses a homogeneous background velocity model suggests topography of the previously imaged positive impedance jump, varying in depth from north to south by as much as 150 km, with a weakly reflecting transition zone in between. The migration approach enables examination of small-scale spatial variations and out-of-plane scattering effects. Topography of the discontinuity may account for observed variations in the amplitude of reflected arrivals or there may be lateral variations in the velocity contrast across the boundary. Lateral variations of the shear velocity structure within the D″ layer may produce some apparent topography in the discontinuity image, but any such volumetric structure is not yet well enough determined to incorporate in the migration. A localized negative impedance contrast reflector or scatterer is imaged at depths about 100 km below the positive reflector in the northern portion of the study area. Several scenarios can explain these results, including (1) a slab that reaches the lowermost mantle, (2) the birth of an upwelling beneath a recumbent slab, or (3) chemical layering in this region. *INDEX TERMS:* 7203 Seismology: Body wave propagation; 7205 Seismology: Continental crust (1242); 7260 Seismology: Theory and modeling; 7299 Seismology: General or miscellaneous; *KEYWORDS:* D″, core-mantle boundary, heterogeneity, lower mantle, shear waves

Citation: Thomas, C., E. J. Garnero, and T. Lay (2004), High-resolution imaging of lowermost mantle structure under the Cocos plate, *J. Geophys. Res.*, *109*, B08307, doi:10.1029/2004JB003013.

1. Introduction

[2] *P* and *S* wave velocity discontinuities have been detected at the top of the D″ region in many areas of the deep mantle (see *Wysession et al.* [1998], *Garnero* [2000], and *Lay and Garnero* [2004] for reviews). Detection of reflections from these discontinuities requires suitable source-receiver configurations, namely, appropriate distance ranges, clean impulsive earthquake source mechanisms, and numerous, high quality recording instruments. D″ discontinuities tend to be strongest in regions of relatively high seismic velocities imaged by seismic tomography [e.g., *Masters et al.*, 2000; *Karason and van der Hilst*, 2001], and may be associated with the onset of transverse isotropy in D″ [*Lay et al.*, 1998a; *Kendall and Silver*, 1998; *Moore et al.*, 2004]. The D″ velocity discontinuity remains a major focus of research since it may hold the key to the origin and nature of the core-mantle boundary (CMB) boundary layer, which appears to play an important role in mantle and core dynamics [e.g., *Lay et al.*, 1998b, 2004a].

[3] The D″ discontinuity structure in the lower mantle beneath Central America and the Caribbean (Figure 1) has been studied over several decades [e.g., *Lay and Helmberger*, 1983; *Zhang and Lay*, 1984; *Kendall and Shearer*, 1994; *Kendall and Nangini*, 1996; *Ding and Helmberger*, 1997; *Reasoner and Revenaugh*, 1999; *Garnero and Lay*, 2003; *Lay et al.*, 2004b]. Most studies

0148-0227/04/2004JB003013$09.00

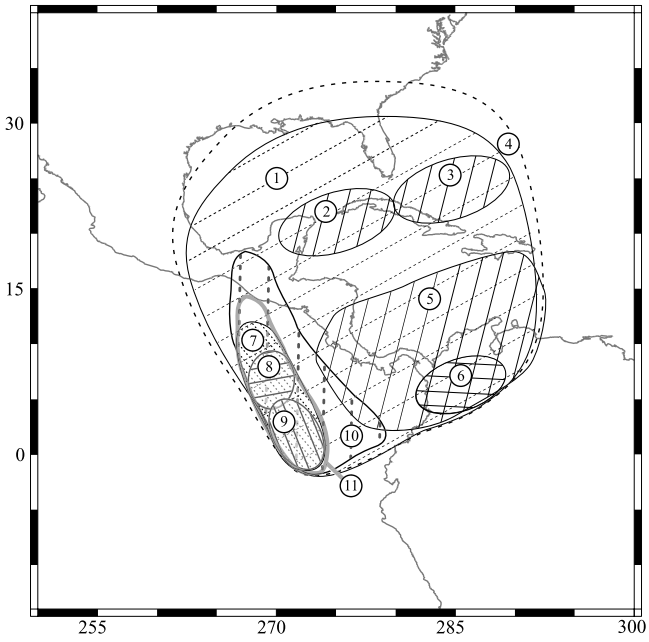

Figure 1. Regions beneath the Caribbean and surrounding areas sampled in previous studies using earthquakes located under South America recorded at seismic stations in North America. Shaded regions and numbers correspond to the specific studies listed in Table 1. The area outlined in gray (region 11) is the study area for this paper.

have utilized *S* waves, finding abrupt shear velocity increases of 2.4 to 3.0% at depths ranging from 180 to 340 km above the CMB (Table 1), as well as localized regions where no reflections are observed. Corresponding discontinuity structure for *P* waves in this region appears to be disproportionately weak or nonexistent (Table 1). The lowermost mantle in this region is characterized by higher than average shear velocities in global tomography models [e.g., *Megnin and Romanowicz*, 2000; *Grand*, 2002]. Attributing high D″ velocities to past subduction is becoming increasingly common in the literature. For example, *Lithgow-Bertelloni and Richards* [1998] predict that ancient subducted Cocos plate should have accumulated in the lower mantle beneath the Caribbean, possibly extending all the way to the CMB [see also *Grand et al.*, 1997]; this could account for the high background velocities and there may be a direct connection to the D″ discontinuity. However; the debate regarding slab penetration all the way to the CMB is still very active [*Anderson*, 2001].

[4] In a recent study, *Lay et al.* [2004b] investigated the shear velocity structure of the D″ region under the Cocos plate (area 11 in Figure 1), using double-array stacking, a method which assumes that all reflections occur in the event station great circle plane, and that there are horizontal reflectors. Using a one-dimensional (1-D) velocity model for the travel time calculations, they find large apparent variations in the discontinuity depth in 4 localized bins. However, their preferred models have a discontinuity uniformly at 264 km above the CMB with laterally varying velocity increase from 0.9% to 2.6% and corresponding variations in the average velocity within the D″ layer. There are significant trade-offs between volumetric heterogeneity and discontinuity topography, as for all imaging methods. Some features in the data were noted to not stack coherently as great circle arrivals, and the uncertain validity of modeling the heterogeneous structure with localized 1-D structures leaves unresolved questions of uniqueness for the resulting models.

[5] Seismic array methods (see *Rost and Thomas* [2002] for a review) offer enhanced spatial resolution and allow for out-of-plane scattering, potentially improving on results from 1-D stacking and modeling approaches. Array processing methods intrinsically seek to determine the incoming direction of signals (i.e., the slowness and back-azimuth) allowing identification of signals originating from lower mantle structures [e.g., *Weber and Davis*, 1990; *Weber*, 1993]. Recently, simplified migration methods have proven to be especially useful in detecting several different classes of D″ structures, ranging from scatterers to discontinuities [e.g., *Lay and Young*, 1996; *Scherbaum et al.*, 1997; *Bilek and Lay*, 1998; *Thomas et al.*, 1999; *Freybourger et al.*, 2001; *Kito and Krüger*, 2001; *Castle and van der Hilst*, 2003a, 2003b; *Thomas et al.*, 2004]. These methods are "simplified" in that they are not formal downward continuations of well-sampled wave fields, rather, most methods are parameterized as kinematic isotropic point scattering inversions. Beneath Eurasia, *Thomas et al.* [2004] used a simplified migration approach to detect two discontinuities (one positive, one negative) in an area where one or two

Table 1. D″ Discontinuity Detection in Our Study Region

Figure 1 Region	Study	*P* or *S*	D″ Thickness, km	Velocity Increase,%	Comments
1	*Lay and Helmberger* [1983]	*S*	250	2.75	thickness variability noted
2	*Kendall and Nangini* [1996]	*S*	290	2.45	
3	*Kendall and Nangini* [1996]	*S*	...	...	no clear discontinuity
4	*Garnero and Lay* [2003]	*S*	...	...	positive discontinuity detections, but not modeled
5	*Kendall and Nangini* [1996]	*S*	250	2.75	
6	*Kendall and Shearer* [1994]	*S*	280	...	magnitude not modeled
7	*Ding and Helmberger* [1997]	*S*	200	3.0	
7	*Ding and Helmberger* [1997]	*P*	...	<1	no evidence found, less than 1% velocity increase possible
8	*Kendall and Shearer* [1994]	*S*	180	...	magnitude not modeled
9	*Zhang and Lay* [1984]	*S*	251	2.71	
10	*Reasoner and Revenaugh* [1999]	*P*	190	0.5–0.6	thickness: ±20 km
11	*Lay et al.* [2004b]	*S*	264	0.9–2.6	four patches under Cocos

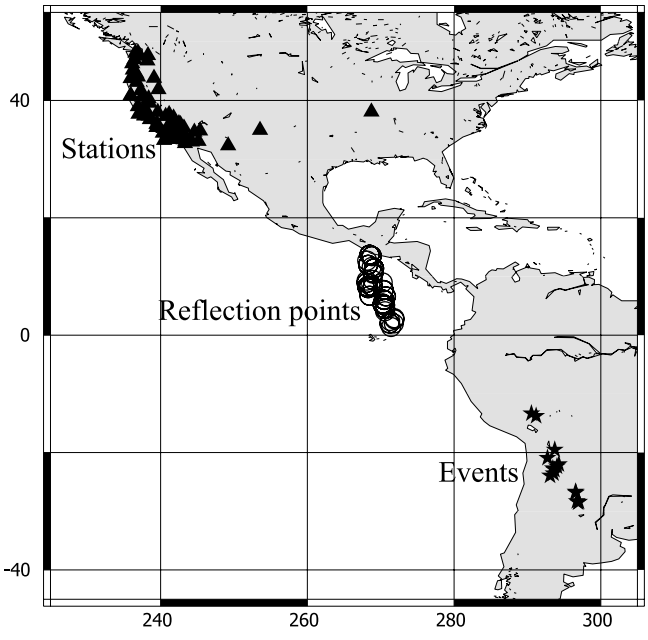

Figure 2. Sources (black stars), receivers (black triangles) and the study area under the Cocos plate (black circles). The circles correspond to *Scd* reflection points in the lowermost mantle. The reflection points are divided into longitudinal bins of 2.5° with an overlap of 1.25°.

positive discontinuities were previously proposed by *Gaherty and Lay* [1992] on the basis of forward modeling of data profiles. In general, if coherent seismic phases arrive at the array out of the great circle plane due to nonplaner reflectors or significant heterogeneity, some form of migration is the most appropriate tool for characterizing the structure, although it remains very difficult to formally model the resulting images. We apply such an approach to provide an alternate parameterization and to improve resolution of the localized shear velocity structure within D″ under the Cocos plate.

2. Data and Processing

[6] We use shear waves from 14 deep earthquakes in the South America subduction zone recorded at Californian broadband network stations from 1993 to 2001 (Figure 2). The processed data are the same as those used by *Lay et al.* [2004b]. Horizontal component records have been deconvolved by the instrument responses to obtain ground displacements, rotated to the great circle reference frame to obtain transverse components of motion (after correction for upper mantle anisotropy effects), deconvolved on an event-by-event basis by the event-averaged *SH* wavelets obtained by stacking all *S* and/or *ScS* observations, and filtered with a low-pass filter (corner of 0.3 Hz). This processing results in filtered spike-trains that are directly comparable in complexity and bandwidth from event to event. Deconvolution noise precludes analysis of frequencies higher than 0.3 Hz in this study. After aligning the signals on *ScS*, the traces are shifted with theoretical *ScS* slowness and back azimuth values to suppress travel time differences from mantle heterogeneities. This effectively establishes the CMB as our reference datum, with the timing of arrivals relative to *ScS* controlling the migration images. Four profiles of deconvolved records for the events of 28 November 1997 (event 9 in Table 2), 15 September 1999 (event 11), 23 April 2000 (event 12), and 10 May 1994 (event 6) are shown in Figure 3 with the traces aligned on *ScS*. Between *S* and *ScS* a clear additional phase can be observed with an intermediate moveout, indicating that this wave was produced by structure in the deep mantle. It is difficult to detect any other arrivals coherent across the entire data set, and there are arrival time fluctuations in the relative timing of the phases at different stations.

[7] A positive D″ shear velocity discontinuity generates such additional arrivals between *S* and *ScS* at teleseismic distances. This additional energy consists of a reflection from the velocity discontinuity and, at postcritical distances, a diving wave turning below the discontinuity (notated as *Sbc* and *Scd*, respectively [*Lay and Helmberger*, 1983]; or *SdS* and *SDS*, respectively [*Weber and Davis*, 1990]). Precritical reflections from a 2–3% velocity increase (typical of the models that have been obtained) tend to be very small, while the *Scd* (*SDS*) arrival is strong at epicentral distances of approximately 70° to 82° [*Wysession et al.*, 1998]. Thus past analyses in this distance range have provided most of the detections of lower mantle shear velocity discontinuities. The slownesses of the additional arrivals are intermediate to the slownesses of *S* and *ScS*. A sharp velocity discontinuity is not uniquely required to produce an additional arrival between *S* and *ScS*, as extra arrivals can also be produced by scattering from strong radial or lateral seismic velocity gradients [*Liu et al.*, 1998] or by a negative velocity lamella [*Thomas et al.*, 1998]. For this reason, most past efforts have utilized distance profiles of data that sample D″ over regional scales (e.g., of order 1000 km laterally) in order to constrain the structure. This intrinsically limits the spatial resolution of studies that use widely distributed stations. We exploit the relatively dense distribution of broadband stations in California to attain improved spatial resolution, with subsets of stations used as array recordings for a given event. With typical 70 km station spacing, the wavefield is still spatially aliased for the 3–8 s predominant periods of our data, so we are limited to simplified migration approaches.

[8] The *ScS* reflection points for our source-receiver combinations span a localized corridor beneath the Cocos

Table 2. Events Used in This Study

Event	Date	Latitude, °S	Longitude, °W	Depth, km
1	23 June 1991	26.82	63.40	558
2	24 May 1993	22.67	66.54	221
3	19 Oct. 1993	22.38	65.97	272
4	10 Jan. 1994	13.339	69.446	596
5	29 April 1994	28.299	63.252	561
6	10 May 1994	28.501	63.096	600
7	19 Aug. 1994	26.642	63.421	564
7	23 Jan. 1997	21.999	65.719	276
8	20 July 1997	22.982	66.301	256
9	28 Nov. 1997	13.74	68.788	586
10	30 Aug. 1999	23.934	66.906	219
11	15 Sep. 1999	20.934	67.275	218
12	23 April 2000	28.384	62.943	609
13	12 May 2000	23.548	66.452	225
14	29 June 2001	19.52	66.25	273

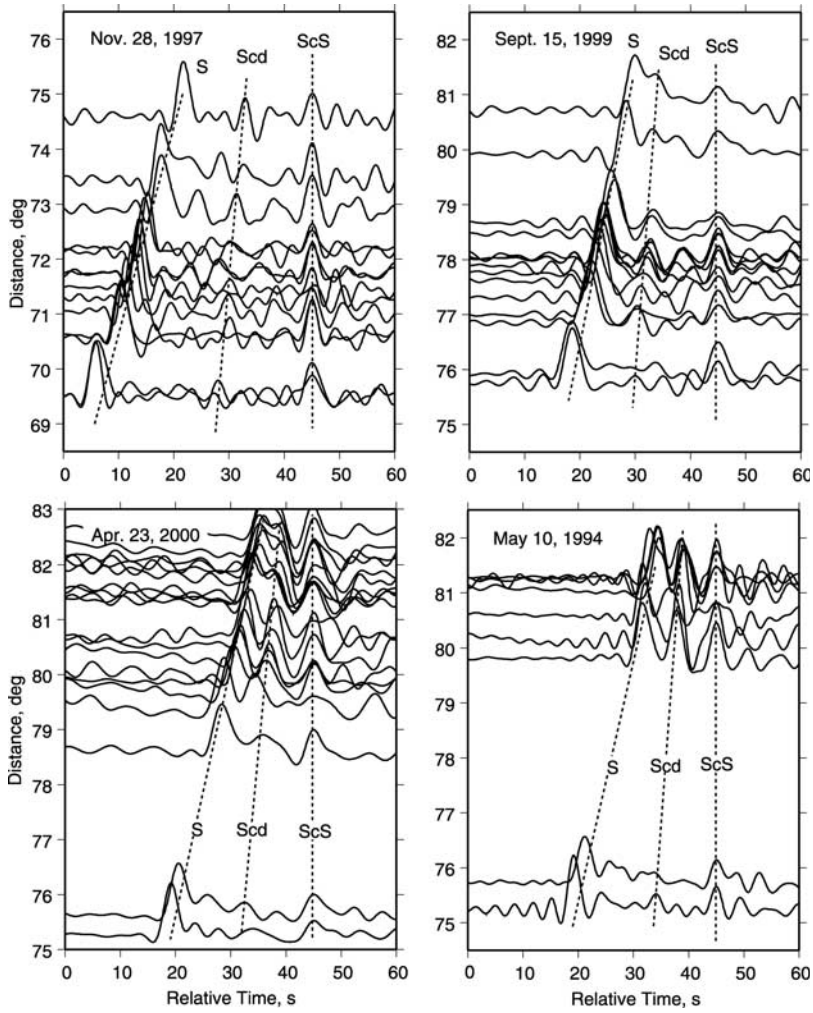

Figure 3. Example data profiles for processed tangential component signals for four events in our data set. The traces are aligned on *ScS*, so times are relative. *S*, *Scd*, and *ScS* arrivals are indicated. The *Scd* phases vary in strength partly because of distance (the arrival increases in amplitude with distance, so it is very strong beyond 79° in the bottom two panels). Note that *Scd* arrives earlier relative to *ScS* in the waveforms for the event of 15 September 1999 than for the two events shown in the bottom panels. The 15 September 1999 event samples the northern half of our study area, while the 23 April 2000 and 10 May 1994 events sample the southern half. These travel time variations are manifested as topography in the D″ reflector imaged by our migrations.

plate from 0° to 15°N and 267° to 273°E (Figure 2). Several studies have reported variable depths and/or amplitudes of D″ reflectors in this area [e.g., *Kendall and Shearer*, 1994; *Kendall and Nangini*, 1996; *Ding and Helmberger*, 1997; *Reasoner and Revenaugh*, 1999; *Ganero and Lay*, 2003; *Lay et al.*, 2004b]. With different reference structures and modeling procedures being used in each study, there remains substantial uncertainty in the properties of the discontinuity. In order to investigate the fine structure, and to avoid averaging out small-scale variations given the prior evidence for lateral heterogeneity, we subdivide our data set into localized spatial bins (2.5° in latitudinal width, i.e., ~160 km) of recordings for individual events. We experiment with overlapping bins as well, leading to 13 latitudinal bins. Since some events sample several bins, and we are using 14 events, we obtain a total of 41 reflection point bins to be investigated. In a first step we produce vespagrams [*Davies et al.*, 1971] for all 41 bins, three of which are shown in Figure 4. Two different regions near 12°N (bin 1) and 3°N (bin 13) are imaged with these vespagrams. The first example is for event 11 in Table 2. For this event *S* arrives with a slowness of 9.5 s/deg at 10 s. *ScS* arrives 20 s after *S* with a lower slowness (~7 s/deg). Both *S* and *ScS* features are clearly visible. In between, the *Scd* arrival is also easily observed, and has a slowness intermediate to *S* and *ScS*. For the second example (event 12 in Table 2 and middle panel in Figure 4), which samples the same bin as the first event, the *Scd* arrival is a bit closer in time to *S* and has a slowness slightly less than that of *ScS*. This may be due to effects of heterogeneity between events or due to *Scd* arriving out of plane, which can severely affect the inferred slowness in a vespagram [*Rost and Thomas*, 2002]. In the third

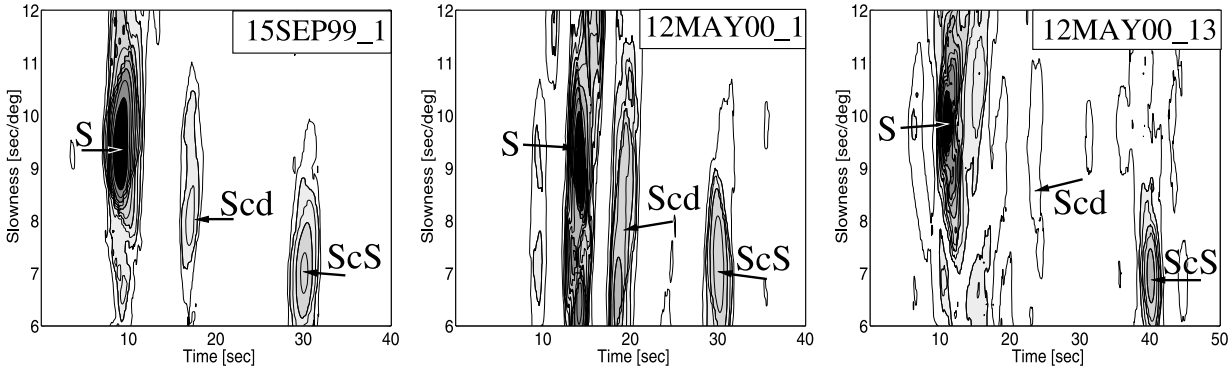

Figure 4. Vespagrams for 3 different source-receiver combinations. The number following the event date indicates the corresponding reflection point bin. In all three examples, the *S* and *ScS* arrivals produce clear energy peaks, at the expected slowness values (arrows). The intermediate arrival *Scd*, produced by the velocity increase at the top of D″, is more variable, with the peak having the expected slowness in the example on the left-hand side, lower slowness than expected in the middle panel, and a very weak arrival on the right-hand panel. The *S* wave is centered at 10 s, and the time axis is relative to *S*.

example (event 12 again, but sampling a bin 13 to the north), *Scd* is less clear than in the other two cases (in fact, it is hardly visible, a combined effect of being at closer distances where triplication effects are less pronounced and the existence of weaker reflection from D″ structure). This variability from bin to bin indicates complexity in the seismic reflector, such as strong topography, or variation in the velocity contrast of the discontinuity. The *Scd* features that we observe in these 1-D vespagrams directly correspond to the energy that is spatially imaged in our 3D migration grids, and there is good agreement for those cases where the signal is strong and involves in-plane arrivals.

[9] To systematically investigate the seismic structure in D″, we apply the simplified migration method used by *Thomas et al.* [1999, 2004]. The data for each bin are slant stacked for a 3-D grid of potential reflectors (or scatterer locations) ranging from −2° to 18°N, 260° to 280°E, with lateral spacing of 1°, and from 2200 to 2888 km depth with vertical spacing of 10 km (thus nearly 30,000 potential reflector locations are investigated for each of the 41 bins of data). The reference model for the travel time computations for *ScS* and for grid point to source and receiver locations is a 1-D mantle shear velocity model ak135 [*Kennett et al.*, 1995]. While use of an aspherical model for travel time computations is plausible, available tomography models are highly variable in their predictions for the very localized structure we sample with our data, so we do not undertake a more ambitious migration in a heterogeneous model at this time. While the east-to-west aperture of our array is limited and there is no crossing coverage, slightly out-of-plane reflections can still be detected, and the grid parameterization potentially allows detection of finer-scale structure compared to one-dimensional stacking or waveform modeling methods of past studies, which use larger pins or longer profiles.

[10] Some reflectors may be weak and not readily detectable in single traces, but through slant stacking they may be clearly observed [e.g., *Krüger et al.*, 1996; *Rost and Revenaugh*, 2003; *Thomas et al.*, 2004]. The advantage of separating the reflection points into latitudinal bins is the enhanced ability to resolve short-scale structure with relatively weak reflectors that might be obscured by velocity heterogeneity otherwise. This fine-scale binning of reflection points becomes robust only when a critical number of data is included in each bin; we found a minimum of seven recordings per bin is necessary to yield stable results for our choice of bins, though, ideally, one would have far larger numbers of recordings in each bin. The threshold for sampling is dependent on the strength of arrivals as well, and lower stability is expected when weak arrivals are present. A similar application of fine-scale reflection points binning is given by *Thomas et al.* [2004]. Use of a small number of traces increases the potential for spurious features to align, giving false images, but confidence in imaged features is gained by redundant sampling by bins of other events. For the current study, events are treated separately, to reduce effects of velocity heterogeneity between events, but multiple-event stacking will be pursued in the future. We have computed reflectivity method [e.g., *Müller*, 1985] synthetic seismogram resolution tests for structures containing and lacking discontinuities, and processed the synthetics in the same way as the data. These experiments always yielded positive discontinuity detection at the appropriate depth, if present in the original model.

[11] One example of a depth section in an individual bin migration is presented in Figure 5. This is the migration of event 11 to a depth in the image grid of 2535 km, at which the amplitude of the stacked and shifted traces is highest and focuses in a small region. The two isolated features northeast and southwest of the main high amplitude region are artifacts from the *ScS* wave, which focuses and forms a coherent reflector deeper, at the CMB. The *Scd* energy, at 2535 km, is spread over an area of 2°–3° in diameter. This is due to the bandwidth limitations of the deconvolved and filtered *S* waves, and the likelihood that this is a specular reflection rather than a point-scattered arrival [e.g., see *Lay and Young*, 1996]. We choose the middle of this region as our discrete reflection point, understanding that we have a spatial spread of approximately 1.5° (∼90 km at the CMB) radially for each reflector detection. The depth resolution is

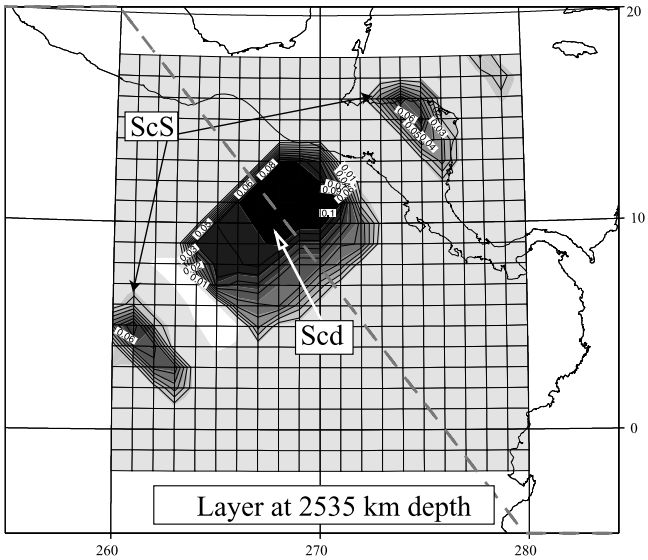

Figure 5. A single depth section of a migration for event 11 (15 September 1999). The most coherent focusing of amplitude of the stacked and shifted traces occurs at this depth of 2535 km in the black region marked as *Scd*. The central contour line is the most likely area of reflection, which yields a zone of approximately 1.5° in latitude and longitude. The *ScS* wave for this event focuses at 2889 km depth (the CMB) and when migrated to shallower depths like this, the *ScS* energy is spread symmetrically to the periphery of the migrated area as indicated [see also *Thomas et al.*, 2004]. The gray dashed diagonal line indicates the great circle path between the source and a station in the center of the Californian broadband networks.

±10 km for our grid, for the assumed homogeneous reference velocity structure.

3. Results

[12] Our analysis provides 41 closely spaced bins in which we may detect coherent arrivals ahead of *ScS* (more than one reflector may be resolved for each bin), illuminating a region beneath the Cocos plate elongated in the north-south direction (Figure 2). Migrating the data in all bins yields a large number of reflector detections, and the results indicate a relatively shallow reflector in the north and a deeper reflector in the south, in general agreement with previous studies [*Lay and Helmberger*, 1983; *Kendall and Shearer*, 1994; *Kendall and Nangini*, 1996]. The depth of the individual reflection points is indicated in Figure 6 by the diameter of the circles, with larger circles indicating a larger distance of the reflector from the CMB. We have used a homogenous velocity model in the migration; however, some tomographic models for the lowermost mantle show an increase in shear velocity from south to north across this region (Figure 6). The southern part of our investigated area approaches the southern edge of the high velocity region in the model of *Grand* [2002], and the *ScS-S* differential times for our data are compatible with this [e.g., *Garnero and Lay*, 2003; *Rokosky et al.*, 2004]. The lack of ray path sampling to the west and south from our study area for all tomographic studies gives large uncertainties in the large-scale velocity gradients across our region, and there are substantial variations between existing models, so we will not attempt to account for small-scale volumetric heterogeneity in our imaging.

[13] The transition zone at latitudes of 5°–8°N between the northern shallower and southern deeper regions of the reflector in Figure 6 is characterized by large variations in the apparent depths of individual reflectors, although the average values follows the trend from shallower to deeper. This scatter may reflect inadequacies of the binning in a rapidly changing region or possibly the decreased amplitude of the *Scd* arrivals in the transition zone, with weaker features being identified as possible coherent arrivals over a range of depths. Some of the *Scd* reflections do appear to be weak in the transition zone (*Garnero and Lay* [2003] note that some signals lack clear *Scd* signals for paths

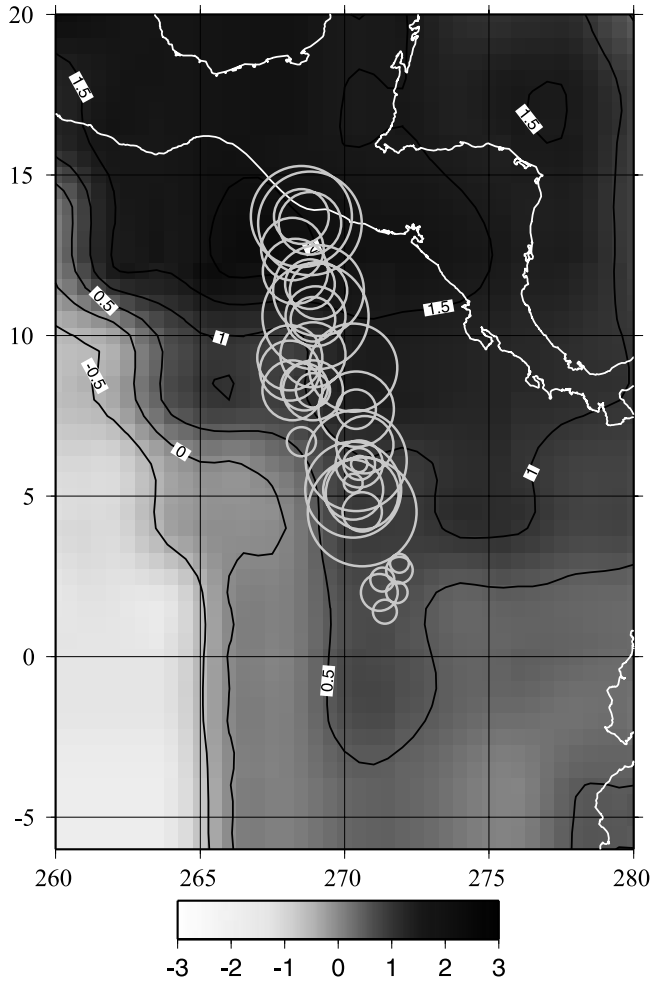

Figure 6. The tomography model of *Grand* [2002] for the lowest layer in the region investigated. The isovelocity lines and gray scale show the velocity contrast δV_S of the model. Superimposed circles are the reflection points for individual bins. The size of each circle corresponds to the distance of the reflector from the CMB. The shallower reflectors coincide with stronger positive volumetric velocity anomalies, the deeper reflector in the south coincides with weaker velocity anomalies in the tomographic image.

turning from 5° to 9°N in latitude, and *Lay et al.* [2004b] find a weak reflector in double-array stacks of data in a bin from 4.5°–7.5°N). Another interesting observation is that, especially in the transitional region, some of the migration reflector detections arrive from positions off the great circle path, again suggesting complexities in reflector structure, such as small-scale topography or scattering. Interaction of the turning wave front with a dipping or undulating surface may lead to highly variable signals from event to event and from bin to bin, which is why we have parameterized the model so finely. Our data lack azimuthal coverage and spatial sampling, so we cannot fully image the structure, and no method is yet available to formally migrate the wavefield amplitudes to better constrain the structure.

[14] In some regions, especially toward the northern area, negative arrivals (with opposite polarity to *S* and *ScS*) are detected. These negative reflections can be identified in individual seismograms (Figure 7), but only intermittently, for their amplitude is generally smaller than the positive reflections. The opposite polarity arrivals in Figure 7 are relatively strong and suggest a moveout different than expected for a simple reflector above the CMB, suggesting out-of-plane scattering. *Lay et al.* [2004b], found that the negative arrivals could not be characterized as in-plane arrivals by double-array stacking, which indicates that for the larger bins used in that study, these phases are not stable over scale lengths of several degrees. The phase-shift of postcritical *Sbc* reflections can produce opposite polarity ground motions soon after *Scd*, complicating the detection of the negative arrivals. Deconvolution sidelobes and receiver noise can also produce negative energy that could stack fortuitously in small data sets. However; being aware of these concerns, we still give credence to coherent negative arrivals in some of our migrations.

[15] In Figure 8, piecewise continuous surfaces interpolating the location of positive and negative reflectors are shown in map view. Any bins with evidence for more than one positive (or negative) reflector have been depth-averaged, and only reflectors below 2500 km depth are considered (above this depth any intermediate arrival is soon after direct *S* in timing, reducing our ability to separately distinguish it, and increasing the potential for contamination by deconvolution sidelobes and artifacts from strong receiver reverberations). The positive reflector exhibits an undulation in the transition zone from shallow (i.e., thick D″) in the north to deep (i.e., thin D″) just to the south, in agreement with the data stacks from the double-array method [*Lay et al.*, 2004b]. The negative reflector is seen in the northern portion of the study area about 100 km below the positive reflector. The kinematics suggest that it has significant horizontal extent, but given that we are using a homogeneous reference model for imaging, we cannot preclude a more concentrated scattering geometry.

[16] The lateral resolution within the north-south corridor of our study is limited due to the source-receiver geometry. However, even within this roughly 150 km wide zone, the results appear stable in the north-south direction: most of the variation in imaged reflector depth appears to be along the ~700 km long corridor. This corresponds to the direction of the significant lateral shear velocity gradient in the background velocity structure (Figure 6), where δV_S in that model is increasing to the north. Since we have aligned our data on *ScS*, regions with D″ velocities that are faster than our reference model will have the discontinuity imaged too shallow in the mantle, whereas slow regions will overestimate the depth of the discontinuity. Some of the topography in our image may be an artifact of lateral gradient in the structure.

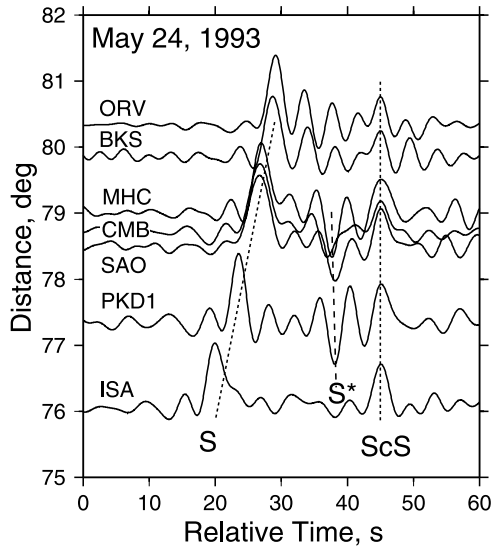

Figure 7. A portion of the data profile for the processed signals from the event of 24 May 1993, with format similar to the profiles in Figure 3. This event samples the central portion of our study area and does not have a clear, large amplitude *Scd* arrival between *S* and *ScS*. However, there is a strong arrival with opposite polarity to *S* and *ScS* apparent in the waveforms of stations MHC, SAO, and PKD1, which moves out with a slowness inconsistent with Scd, suggestive of an out-of-plane scattered arrival from above the CMB. This feature is observed intermittently in the central and northern portion of our study area, and migration is needed to image the scattering region.

[17] Figure 9 shows three-dimensional plots of the piecewise continuous surface with a lateral decimation of 0.5°. The individual reflection points for the positive velocity increase project close to the upper, smoothed positive reflector surface, indicating that the apparent reflector position is well constrained for the given velocity model. This is especially so in the north and south, but in the transition zone the deviation from the smoothed surface is much stronger (Figure 9). To further illustrate that there is less variance of estimated reflector depths toward the northern and southern ends of our corridor, the average and standard deviation of the imaged high-velocity reflector depths are plotted versus latitude in Figure 10 (±1 standard deviation about the average is shown by the vertical lines). While the total population of reflection points is not large, there is a clear suggestion that the spread of reflection depths is greatest in the middle of the transition zone (between 5° and 8°N) where the *Scd* arrivals are weak. This is partly due to some events exhibiting more than one positive reflector in the transition zone. All the individual reflector depths have been used in producing the reflector surface of Figure 8 (left) and 9; however, it is possible that the shallowest reflections (less

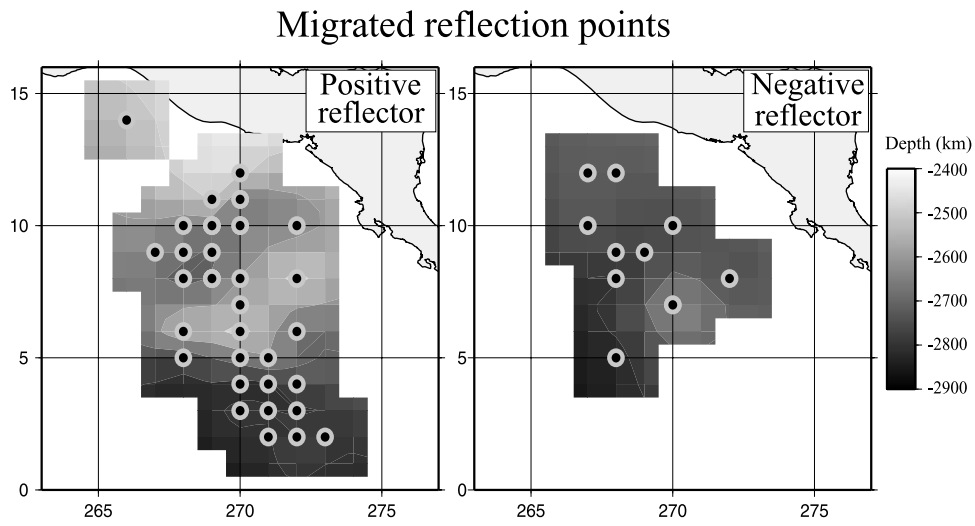

Figure 8. Map view of two reflectors with averaging of the individual results. The positive reflector is given on the left-hand side, and the negative reflector is given on the right-hand side. The gray scale indicates the depth of the reflectors. The positive reflector exhibits a trend from a higher region (2500 km deep) in the north via a transitional region to approximately 2800 km deep in the south. In the transition region, undulations of the reflector can be noticed. The negative reflector is only seen in the area north of 5°N, and the distance from the CMB increases toward the north. The black/gray circles indicate the migrated reflection points for the middle of the migrated area.

than 2550 km deep) might be due to scattering above our principle layer of interest (that is, the likely surface of D″), or they could be associated with a separate positive velocity increase layer above the upper reflector surface in these images. There is some potential for the shallowest features to be fortuitous images formed from strong receiver reverberations in the data, so we downweight their importance.

[18] It is instructive to attempt to extract intermediate wavelength patterns in our reflector depth estimates. Figure 11 shows the velocity increase and velocity decrease reflectors as continuous surfaces in a 3D image (the top and bottom sheet, respectively). Here, the migrated reflector depths have been averaged in 2° × 2° bins, then fit with a best fitting surface of moderate tension. The smoothing may over emphasize lateral continuity of the structure, but the kinematics of the data behavior can be quite well represented with these smoothed models. The negative (lower) reflector follows the depth-trend of the positive (upper) one where they both are resolved. This provocative image emphasizes the general apparent thickening of the D″ toward the north, with a complex gradient from a thinner layer to the south. It is important to recognize that this undulating pattern is for the image formed in a homogeneous velocity model, and introduction of volumetric velocity variations below either discontinuity will directly trade off with the depth estimate for that discontinuity. The data attribute not explicitly accounted for in the simplified migration method is the amplitude of the reflected/scattered waves; the rough apparent topography would cause amplitude variations for *Scd*, and may be consistent with the data (the large bump in the upper surface

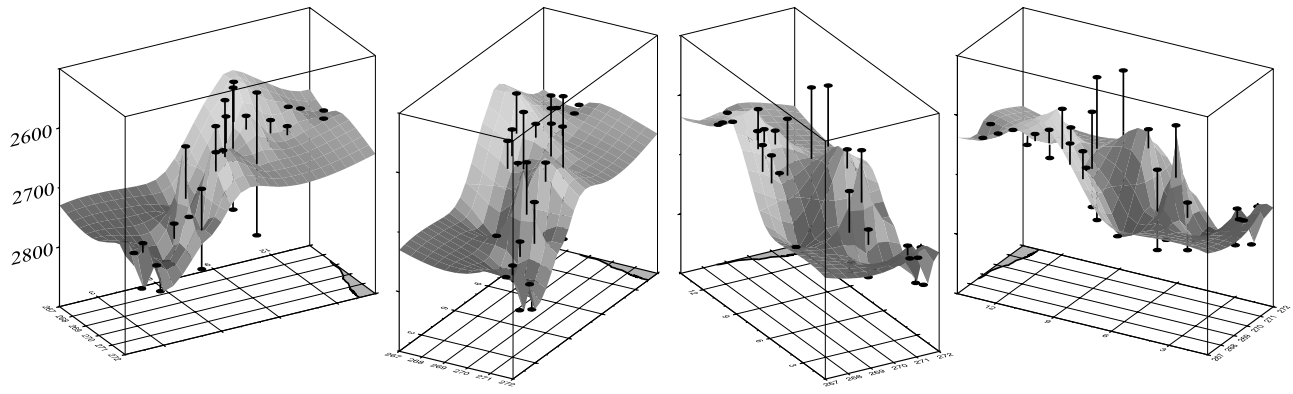

Figure 9. Four views (looking to the north) of the surface of the upper positive reflector with the individual reflection points superimposed. The average surface is well constrained in the north and south as the individual data plot close to the surface; in the transition zone the reflector depths are more scattered so the average surface is less reliable.

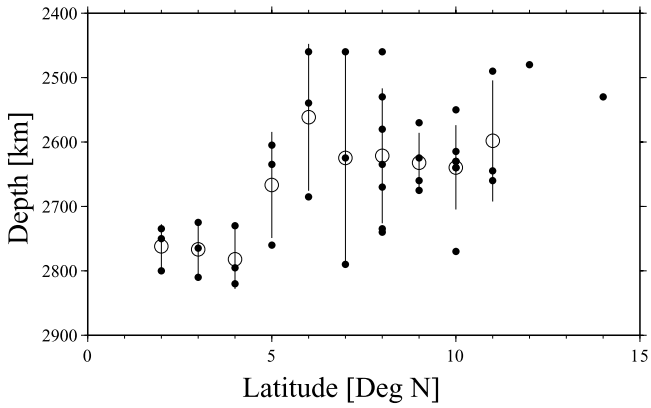

Figure 10. The individual bin estimates of reflection depth (black circles), average reflector depth (white circles) and 1 standard deviation (black lines) for the positive reflector in a two-dimensional plot where reflection points have been averaged in 1° bins in latitude. The *y* axis shows depth. The spread is greatest in the middle, and the standard deviations are much smaller in the south and in the north of the studied region.

could account for the weak observed *Scd* arrivals). Figure 11 is a purely kinematic image based on the relative timing of coherent features relative to the CMB reflections for a homogenous background model.

4. Interpretation

[19] Our migration results suggest strong topographic variations on a positive reflector, generally deepening from north to south, with a complex transition zone in between. The transition zone has weak *Scd* arrivals and is marked by scatter in imaged topography, more than one reflector image, and out of plane reflections, all of which could be noise effects due to weakness of the *Scd* energy. In addition a negative reflector is observed in the northern region (north of 5°N) below the principal positive velocity jump surface, with a depth variation that seems to follow the trend of the upper reflector. We emphasize that the topographic undulations are just apparent, in that the depth estimates are entirely dependent upon the assumption of homogeneous 1-D reference structure. It is notable that *Lay et al.* [2004b] can reproduce similar apparent depth variations in stacked images by allowing for lateral variation in velocity below a uniform depth discontinuity. Determination of a suitable regional-scale tomographic model of the volumetric velocity structure in the future would allow migrations with an aspherical model that would help resolve this trade-off. For this study we simply keep in mind the associated trade-offs which are intrinsic to all imaging methods.

[20] Figure 12 shows four possible explanations for the complex structure found in our study. The first possibility (Figure 12a) is that subducted lithosphere, in this case ancient Farallon plate, descends toward the CMB, possibly not quite reaching it. In the lower mantle it could buckle or fold as the convection models of *Christensen and Hoffman* [1994]. For this case, the upper, positive reflection can perhaps be explained by thermal and chemical gradients near the top of the slab in the deep mantle, the negative reflector would then be from the lower boundary of the slab. This explanation parallels that favored by *Thomas et al.* [2004], who find that migration of synthetic data derived

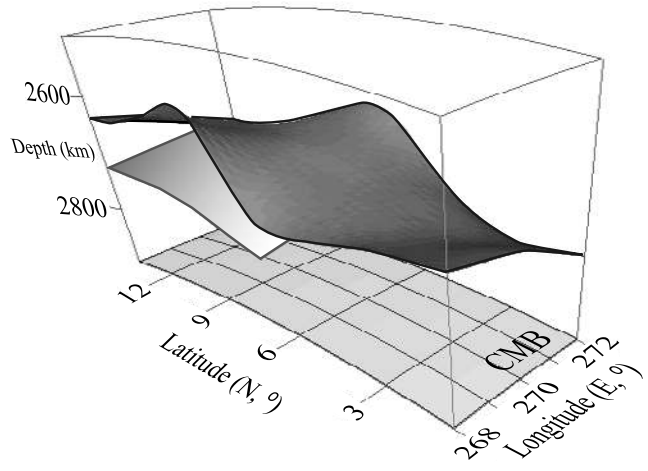

Figure 11. The positive (top) and negative (bottom) reflecting surfaces, smoothed and plotted in three dimensions relative to each other. The negative reflector is not detected in the southern region and in the northern region it follows the main trend of the upper positive reflector.

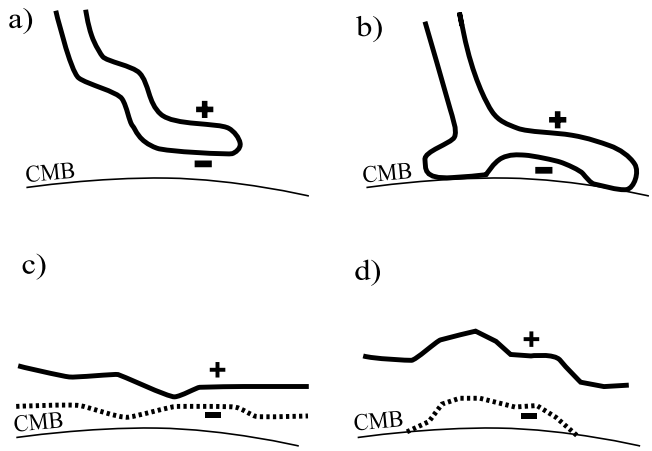

Figure 12. Four candidate scenarios to explain the observations of two reflectors. (a) High velocity subducted lithosphere of the Farallon plate that has descended to the bottom part of the mantle. The positive reflector indicates the top of the slab; the negative reflector indicates the bottom of the slab. (b) The birth of an upwelling. The subducted lithosphere has reached the CMB and at its underside material heats up, eventually producing an upwellings [*Tan et al.*, 2002]. (c) The observation of both reflectors can be attributed to layering of a thermochemical boundary layer, the upper layer might indicate the top of the chemical layer, and the negative reflector could be an internal low velocity zone associated with partial melting within the layer. (d) The lower reflector might not be continuous as indicated in Figure 12c but localized.

from a geodynamic model can explain positive and negative reflectors seen in a lowermost mantle region beneath Eurasia. Whether it is viable to have thermal and chemical gradients strong enough to produce the seismic wave triplications remains a controversial topic [e.g., *Sidorin et al.*, 1999]. A second possibility is shown in Figure 12b. In this case the slab has reached and accumulated at the CMB. At its underside, between the core and the slab, material heats up and possibly forms an instability that may evolve into a future upwelling. Geodynamic modeling by *Tan et al.* [2002] has shown that this scenario is one of the possible birthplaces for hot upwellings. This scenario has been advanced to account for a region to the east of our study area, just north of Venezuela [*Wysession et al.*, 2001; *Fisher et al.*, 2003]. Figure 12c assumes a thermochemical boundary layer at the top of the core without the influence of a slab. This boundary layer could exhibit internal layering and/or heterogeneities, hence producing the observed reflectors seen in the data. *Lay et al.* [2004a] suggest the possibility of a global thermochemical boundary layer with laterally varying amounts of partial melting. This explanation could include a low-velocity lamella, which has been shown to generate a similar seismic signal to a positive reflector [*Thomas et al.*, 1998] or even stacks of lamellae [*Moore et al.*, 2004], which have been shown to generate anisotropy as observed in some high velocity regions in the lowermost mantle. Certainly, lateral variations in some partial melt component to D″ might be expected (as in Figure 12d).

[21] Our results for the lowermost mantle beneath the Cocos plate suggest significant complexity in the seismic structure; however, they do not allow us to discriminate between the scenarios given in Figure 12. The data clearly establish the presence of lateral variations in the depth and/or strength of the shear velocity increase at the top of the D″ layer, and the possibility of substantial topography on this discontinuity. We also find evidence for strong negative arrivals associated with scattering in the northern portion of our study area. More information is needed, especially concerning the lateral extent of the reflectors to the west and south, to determine whether the positive reflector is associated with high velocity regions of D″ only. In addition, further analysis with *P* waves is needed to determine whether the observed shear wave structure has a *P* wave counterpart. In recent D″ region studies, the observed *P* and *S* wave structures may be significantly different for a given region [*Wysession et al.*, 1998]. At present, *P* wave studies in the area beneath the Cocos plate give conflicting evidence for D″ structure; a deep reflector varying in depth from 162 to 218 km above the CMB with variable *PdP*/*P* amplitude ratios spanning a factor of 1.7 has been proposed [*Reasoner and Revenaugh*, 1999]. However in an overlapping region at the southern end of our study area, no observation of a *P* wave reflector has been made [*Mori and Helmberger*, 1995; *Ding and Helmberger*, 1997]. It appears that at a minimum, the velocity increase for *P* is much less than that for *S*, if a *P* velocity increase is present at all.

[22] Seismic anisotropy consistent with transverse isotropy is present throughout the corridor studied in this paper [*Rokosky et al.*, 2004], with relatively uniform splitting of *ScS* by about 1 s. The transition region in our image does appear to have a slight reduction in shear wave splitting, but this is a subtle effect. The anisotropic observations do not yet help to discriminate between scenarios, but there is potential for this if improved depth resolution on the anisotropy can be obtained. *Rokosky et al.* [2004] observe some splitting of *Scd*, smaller in magnitude than seen for *ScS*, which may lead to improved constraints in future work.

5. Conclusion

[23] Fourteen South American earthquakes have been analyzed using a migration method to investigate the seismic velocity structure in a localized region of D″ beneath the Cocos plate. In contrast to prior methods, our simplified migration approach allows us to consider more localized structures and out-of-plane scattering effects. We find evidence for a regionally extensive positive impedance reflector, with strong apparent topography with increasing depth toward the south, ranging from around 300 to 150 km above the CMB. A second, negative reflector or scatterer has been found north of 5°N following the main trend of the positive upper reflector. The apparent depth of the negative reflector ranges from 180 to 80 km above the CMB and its spatial configuration is ill constrained. It appears to be more of a scattering interface than a stratification. If there is velocity heterogeneity within the D″ region across our small study area, the apparent topography may be underestimated or overestimated. Possible explanations for the features that are imaged include reflections from the top and bottom of a dipping slab; a recumbent slab with an underlying low-velocity zone, possibly a future upwelling; as well as layering within a partially melted thermochemical boundary layer. Future efforts utilizing larger arrays, multievent migration procedures, migration in heterogeneous models, and synthetic modeling approaches with 2-D and 3-D wave propagation simulations will help to distinguish between a number of viable dynamical scenarios that give rise to our observations.

[24] **Acknowledgments.** We would like to thank Klaus Stammler for his data analysis program Seismic Handler. All maps were produced with GMT [*Wessel and Smith*, 1991]. We thank Jeroen Ritsema, Don Helmberger, and Michael Wysession for helpful comments on the manuscript. C. T. was partly supported by RDF grant 4215. E. Garnero was supported by NSF grant EAR-0135119 and T. Lay was supported by NSF grant EAR 0125595. J. Polet provided helpful information about lithospheric anisotropy corrections for our data. M. Simkin constructed Figure 11 using HoloDraw (available at http://holodraw.org). Data were obtained from the Berkeley Digital Seismic Network, TRInet/Terrascope Seismic Network, and IRIS Global Seismic Network, via the IRIS Data Management Center.

References

Anderson, D. L. (2001), Top-down tectonics?, *Science*, *293*, 2016–2018.

Bilek, S. L., and T. Lay (1998), Lower mantle heterogeneity beneath Eurasia imaged by parametric migration of shear waves, *Phys. Earth Planet. Inter.*, *108*, 201–218.

Castle, J. C., and R. D. van der Hilst (2003a), Searching for seismic scattering off mantle interfaces between 800 km and 2000 km depth, *J. Geophys. Res*, *108*(B2), 2095, doi:10.1029/2001JB000286.

Castle, J. C., and R. D. van der Hilst (2003b), Using ScP precursors to search for mantle structures beneath 1800 km depth, *Geophys. Res. Lett.*, *30*(8), 1422, doi:10.1029/2002GL016023.

Christensen, U. R., and A. W. Hofmann (1994), Segregation of subducted oceanic crust in the convecting mantle, *J. Geophys. Res.*, *99*, 19,867–19,884.

Davies, D., E. J. Kelly, and J. R. Filson (1971), Vespa process for analysis of seismic signals, *Nature Phys. Sci.*, *232*, 8–13.

Ding, X. M., and D. V. Helmberger (1997), Modeling D″ structure beneath Central America with broadband seismic data, *Phys Earth Planet. Inter.*, *101*, 245–270.

Fisher, J. L., M. E. Wysession, and K. M. Fischer (2003), Small-scale lateral variations in D″ attenuation and velocity structure, *Geophys. Res. Lett.*, *30*(8), 1435, doi:10.1029/2002GL016179.

Freybourger, M., S. Chevrot, F. Krüger, and U. Achauer (2001), A waveform migration for the investigation of *P* wave structure at the top of D″ beneath northern Siberia, *J. Geophys. Res.*, *106*, 4129–4140.

Gaherty, J. B., and T. Lay (1992), Investigation of laterally heterogeneous shear velocity structure in D″ beneath Eurasia, *J. Geophys. Res.*, *97*, 417–435.

Garnero, E. J. (2000), Lower mantle heterogeneity, *Annu. Rev. Earth Planet. Sci.*, *28*, 509–537.

Garnero, E. J., and T. Lay (2003), D″ shear velocity heterogeneity, anisotropy and discontinuity structure beneath the Caribbean and Central America, *Phys. Earth Planet. Inter.*, *140*, 219–242.

Grand, S. P. (2002), Mantle shear wave tomography and the fate of subducted slabs, *Philos. Trans R. Soc. London, Ser. A*, *360*, 2491–2575.

Grand, S. P., R. D. van der Hilst, and S. Widiyantoro (1997), Global seismic tomography: A snapshot of convection in the Earth, *GSA Today*, *7*, 1–7.

Kárason, H., and R. D. van der Hilst (2001), Tomographic imaging of the lowermost mantle with differential times of refracted and diffracted core phases PKP, Pdiff, *J. Geophys. Res.*, *106*, 6569–6587.

Kendall, J.-M., and C. Nangini (1996), Lateral variations in D″ below the Caribbean, *Geophys. Res. Lett.*, *23*, 399–402.

Kendall, J.-M., and P. M. Shearer (1994), Lateral variations in D″ thickness from long period shear wave data, *J. Geophys. Res.*, *99*, 1575–1590.

Kendall, J.-M. and P. G. Silver (1998), Investigating causes of D″ anisotropy, in *The Core-Mantle Boundary Region*, *Geodyn. Ser.*, vol. 28, edited by M. Gurnis et al., pp. 97–118, AGU, Washington, D. C.

Kennett, B. L. N., E. R. Engdahl, and R. Buhland (1995), Constraints on seismic velocities in the Earth from travel-times, *Geophys. J. Int.*, *122*, 108–124.

Kito, T., and F. Krüger (2001), Heterogeneities in D″ beneath the southwestern Pacific inferred from scattered and reflected *P*-waves, *Geophys. Res. Lett.*, *28*, 2545–2548.

Krüger, F., F. Scherbaum, M. Weber, and J. Schlittenhardt (1996), Analysis of asymmetric multipathing with a generalization of the double-beam method, *Bull. Seismol. Soc. Am.*, *86*, 737–749.

Lay, T., and E. J. Garnero (2004), Core-mantle boundary structures and processes, in *Geophysical Monograph Series*, edited by R. S. J. Sparks and C. J. Hawkesworth, AGU, Washington, D. C., in press.

Lay, T., and D. V. Helmberger (1983), A lower mantle *S*-wave triplication and the shear velocity structure of D″, *Geophys. J. R. Astron. Soc.*, *75*, 799–837.

Lay, T., and C. J. Young (1996), Imaging scattering structures in the lower mantle by migration of long-period *S* waves, *J. Geophys. Res.*, *101*, 20,023–20,040.

Lay, T., Q. Williams, E. J. Garnero, L. Kellogg, and M. E. Wysession (1998a), Seismic wave anisotropy in the D″ region and its implications, in *The Core-Mantle Boundary Region*, *Geodyn. Ser.*, vol. 28, edited by M. Gurnis et al., pp. 299–318, AGU, Washington D. C.

Lay, T., Q. Williams, and E. J. Garnero (1998b), The core-mantle boundary layer and deep Earth dynamics, *Nature*, *392*, 461–468.

Lay, T., E. J. Garnero, and Q. Williams (2004a), Partial melting in a thermo-chemical boundary layer at the base of the mantle, *Phys. Earth Planet. Inter.*, in press.

Lay, T., E. J. Garnero, and S. A. Russell (2004b), Lateral variation of the D″ discontinuity beneath the Cocos plate, *Geophys. Res. Lett.*, L15612, doi: 10.1029/2004GL020300.

Lithgow-Bertelloni, C., and M. A. Richards (1998), The dynamics of Cenozoic and Mesozoic plate motions, *Rev. Geophys.*, *3i6*, 27–78.

Liu, X.-F., J. Tromp, and A. M. Dziewonski (1998), Is there a first-order discontinuity in the lowermost mantle?, *Earth Planet. Sci. Lett.*, *160*, 343–351.

Masters, G., H. Bolton, A. M. Dziewonski, and G. Laske (2000), The relative behavior of shear velocity, bulk sound speed, and compressional velocity in the mantle: Implications for chemical and thermal structure, in *Earth's Deep Interior: Mineral Physics and Tomography From the Atomic to the Global Scale*, *Geophys. Monogr. Ser.*, vol. 117, edited by S. Karato et al., pp. 63–87, AGU, Washington, D. C.

Mégnin, C., and B. Romanowicz (2000), The 3D shear velocity structure of the mantle from the inversion of body, surface and higher mode waveforms, *Geophys. J. Int.*, *143*, 709–728.

Moore, M. M., E. J. Garnero, T. Lay, and Q. Williams (2004), Shear wave splitting and waveform complexity for lowermost mantle structures with low-velocity lamellae and transverse isotropy, *J. Geophys. Res.*, *109*, B02319, doi:10.1029/2003JB002546.

Mori, J., and D. V. Helmberger (1995), Localized boundary layer below the mid-Pacific velocity anomaly identified from a *PcP* precursor, *J. Geophys. Res.*, *100*, 20,359–20,365.

Müller, G. (1985), The reflectivity method: A tutorial, *J. Geophys.*, *58*, 153–174.

Reasoner, C., and J. Revenaugh (1999), Short-period *P* wave constraints on D″ reflectivity, *J. Geophys. Res.*, *104*, 955–961.

Rokosky, J., T. Lay, E. J. Garnero, and S. A. Russell (2004), High-resolution investigation of shear wave anisotropy in D″ beneath the Cocos plate, *Geophys. Res. Lett.*, *31*, L07605, doi:10.1029/2003GL018902.

Rost, S., and J. Revenaugh (2003), Small-scale ultralow-velocity zone structure imaged by *ScP*, *J. Geophys. Res.*, *108*(B1), 2056, doi:10.1029/2001JB001627.

Rost, S., and C. Thomas (2002), Array seismology: Methods and application, *Rev. Geophys.*, *40*(3), 1008, doi:10.1029/2000RG000100.

Scherbaum, F., F. Krüger, and M. Weber (1997), Double beam imaging: Mapping lower mantle heterogeneities using combinations of source and receiver arrays, *J. Geophys. Res.*, *102*, 507–522.

Sidorin, I., M. Gurnis, and D. V. Helmberger (1999), Dynamics of a phase change at the base of the mantle consistent with seismological observations, *J. Geophys. Res.*, *104*, 15,005–15,023.

Tan, E., M. Gurnis, and L. Han (2002), Slabs in the lower mantle and their modulation of plume formation, *Geochem. Geophys. Geosyst.*, *3*(11), 1067, doi:10.1029/2001GC000238.

Thomas, C., M. Weber, A. Agnon, and A. Hofstetter (1998), A low-velocity lamella in D″, *Geophys. Res. Lett.*, *25*, 2885–2888.

Thomas, C., M. Weber, C. Wicks, and F. Scherbaum (1999), Small scatterers in the lower mantle observed at German broadband arrays, *J. Geophys. Res.*, *104*, 15,073–15,088.

Thomas, C., J.-M. Kendall, and J. P. Lowman (2004), Lower-mantle seismic discontinuities and the thermal morphology of subducted slabs, *Earth Planet. Sci. Lett.*, in press.

Weber, M. (1993), *P*- and *S*-wave reflections from anomalies in the lower mantle, *Geophys. J. Int.*, *115*, 183–210.

Weber, M., and J. P. Davis (1990), Evidence of a laterally variable lower mantle structure from *P*- and *S*-waves, *Geophys. J. Int.*, *102*, 231–255.

Wessel, P., and W. H. F. Smith (1991), Free software helps map and display data, *Eos Trans. AGU*, *72*(441), 445–446.

Wysession, M. E., T. Lay, J. Revenaugh, Q. Williams, E. J. Garnero, R. Jeanloz, and L. H. Kellogg (1998), The D″ discontinuity and its implications, in *The Core-Mantle Boundary Region*, *Geodyn. Ser.*, vol. 28, edited by M. Gurnis et al., pp. 273–297, AGU, Washington D. C.

Wysession, M. E., K. M. Fischer, G. I. Al-Eqabi, P. J. Shore, and I. Gurari (2001), Using MOMA broadband array *ScS-S* data to image smaller-scale structures at the base of the mantle, *Geophys. Res. Lett.*, *28*, 867–870.

Zhang, J., and T. Lay (1984), Investigation of a lower mantle shear-wave triplication using a broadband array, *Geophys. Res. Lett*, *11*, 620–623.

E. J. Garnero, Department of Geological Sciences, Arizona State University, Box 871404, Tempe, AZ 85287-1404, USA. (garnero@asu.edu)

T. Lay, Earth Sciences Department and Institute of Geophysics and Planetary Physics, University of California, Santa Cruz, CA 95064, USA.

C. Thomas, Department of Earth and Ocean Sciences, University of Liverpool, Liverpool L69 3GP, UK.